

Mechanical and Electrical Properties of Single Molecules

Thilo Glatzel

Abstract Molecular systems and devices are an strongly emerging technology. Various devices are already available, while others are still under development. The usage of molecules offers a great advantage to Si-based electronics, the functional groups of the molecules are adoptable allowing to artificially generate a huge variety of different properties and functionalities. However, the fundamental requirements of molecular engineering are not fully developed yet, mainly well-known molecules with limited functionality are used nowadays. To analyze and create new molecular structures providing, for example, a very high extinction coefficient while maintaining the chemical structure under environmental conditions would allow to create new types of solar cell conversion devices. This chapter introduces and reviews the research activities of the Nanolino-group at the University of Basel in the active field of the usage of scanning probe microscopy techniques to characterize the mechanical and electrical properties of molecular assemblies down to single molecules.

Keywords Scanning probe microscopy • Single molecules • Molecular assemblies • Insulators • KBr • NaCl

1 Introduction

Molecular electronics is based on the ultimate goal to use single molecules in electronic devices [1–3]. A major challenge is to mechanically stabilize and electrically decouple the molecules at and from a surface, respectively. Unfortunately, these requirements are somehow contradictory, while most molecular assemblies and single-molecular studies are done on metallic surfaces by scanning tunneling microscopy (STM) [4–6], the electrically decoupling requires insulating films or

T. Glatzel (✉)

Department of Physics, University of Basel, Klingelbergstr. 82, 4056 Basel, Switzerland
e-mail: thilo.glatzel@unibas.ch

substrates. Controlled growth procedures of single molecules on insulators are often hindered by the weak, unspecific interactions between molecules and insulating surfaces, which leads to surface diffusion and assembly of disordered aggregates. Furthermore, insulating substrates require characterization approaches, which are rather independent of the conductivity. One way is the usage of ultra-thin insulating films which was shown to allow even orbital imaging by low-current STM [7]. An alternative way is the usage of non-contact atomic force microscopy (nc-AFM) [8], which cannot only image molecules on insulating films or bulk insulator surfaces but is also able to determine mechanical and electrical properties at the submolecular scale, e.g., [9–16]. Even vertical and horizontal manipulation processes as well as measurements of single molecules on insulating surfaces at room temperature are possible [17–21]. This process might also be important for molecular electronics since molecules have to be arranged or contacts have to be moved to the molecules. In a seminal work, Gross and co-workers [22] demonstrated that nc-AFM is not only able to image single atoms and molecules, but is also able to detect the charge state of adatoms on thin insulating films. The authors used bias spectroscopy measurements related to Kelvin probe force microscopy (KPFM) [23–25] and determined the so-called local contact potential difference (LCPD) [26].

The achievements in scanning probe microscopy have tremendous consequences for the field of molecular electronics [27]. Molecules can now be imaged down to the submolecular level; even on insulating substrates, single metal atoms can be manipulated to certain positions and act as electrical contact to the molecule; and finally, the electrical and mechanical properties can be determined also under external excitation. Figure 1 summarizes and illustrates these advances. As shown in the figure, the AFM tip or an external excitation can alter the charge state of the

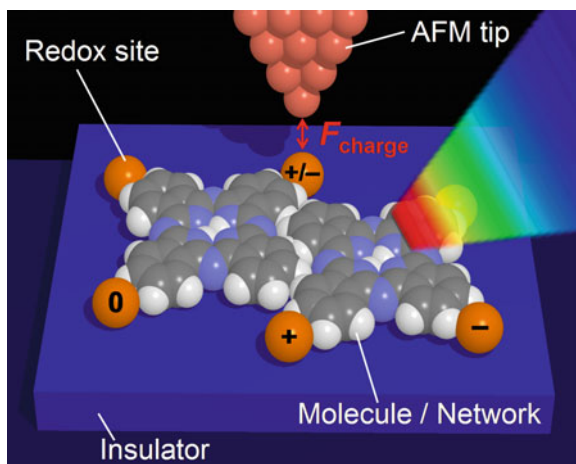


Fig. 1 A single molecule or molecular network on an insulator can be probed by the attachment of metallic adatoms, where single electron charges can be excited by incident photons. Subsequently, the charge transport can be investigated by the measurement of charge states of all the terminal adatoms or directly within the molecule by scanning probe microscopy. Image adopted from [27]

molecule which can afterward be measured by the change of the charge states of the others terminals. This leads to a direct insight into the energy adsorption and propagation of charges in the molecule or a molecular network. Such a change of the charge state of a molecule is in principle an artificial way of a local chemical reduction or oxidation process. Just recently, local Raman scattering measurements at submolecular scale have been demonstrated [28].

In this chapter, the results in the field of advanced atomic force microscopy for high-resolution detection and manipulation of single molecules done at the University of Basel in the Nanolino-group [29] are summarized and discussed. Started some years ago, porphyrin-type molecules were functionalized to allow the stable adsorption of molecular assemblies on alkali halide surfaces (Sect. 2). The formation, manipulation and even the contacting of such wires by non-contact atomic force microscopy (nc-AFM) at room temperature were studied [11, 24, 30–33]. Finally, even a single truxene molecule could be stabilized at room temperature on a KBr surface at a step edge [34, 35]. Section 3 summarizes results acquired by low-temperature combined nc-AFM and STM measurements. At low temperatures, the mobility of the molecules can be reduced so that local elasticity, manipulation, and finally also the determination of electrostatic properties (Sect. 4) are possible [36–43].

2 Porphyrin-Based Molecular Assemblies

π -conjugated molecules such as porphyrins with tunable electronic properties are appealing building blocks for the construction of functional materials with exceptional electrochemical and photophysical properties [44]. All porphyrins absorb light in the visible range and therefore appear colored and are interesting candidates for photovoltaic applications [45]. The chemical structure of a porphyrin molecule is based on a macrocycle having four pyrrole rings cyclic linked by four methyne groups to build an extended aromatic π -system with 18 π -electrons per core. The core has a fourfold symmetry and can be augmented with functional groups in many ways. Furthermore, the two hydrogen atoms in the middle can be substituted by a metal atom (e.g., Fe, Mg, and Zn, ...) having profound influence on the electrochemical activity. This might also explain why porphyrin molecules are very crucial building blocks in nature, e.g., the most important ones are involved in photosynthesis and the transport of oxygen. In the metabolism of mammals, oxygen is transported by red blood cells, the hemoglobin. The major part of it is the HEME group, an iron-(II)-substituted porphyrin. The photosynthesis taking place in plants uses chlorophylls which are magnesium-(II)-chlorin complexes with chlorin being a porphyrin derivate. To allow photosynthesis, the porphyrins absorb red light which is responsible for the green color of all plants [44].

The growth of ordered molecular structures on insulators was in the beginning limited due to a lack of well-adapted molecules. By developing specific cyanophenyl end groups and link them to the porphyrin core [46], these could be solved. In the following, structural, mechanical, and electrical measurements of well-ordered

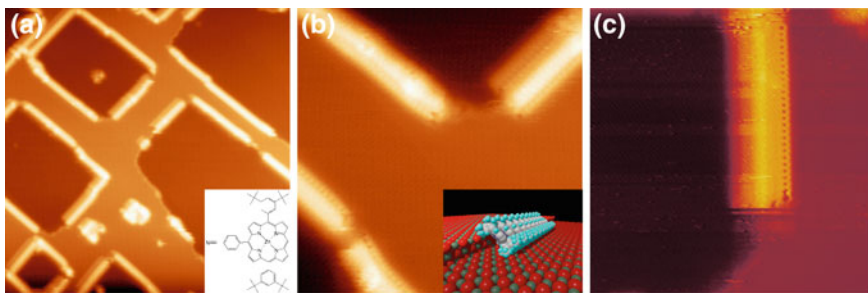


Fig. 2 **a** nc-AFM measurement of single atomic KBr step edges decorated with cyanoporphyrin molecules (*inset*), size = $100 \times 100 \text{ nm}^2$. **b** Wire-like molecular structures which are stabilized by an intermolecular interaction (π - π stacking) and directed electrostatic interaction with the alkali halide substrate. **c** A high-resolution nc-AFM measurement (size = $22 \times 22 \text{ nm}^2$) shows single-molecular resolution, while some molecules are already removed from the wire [30]

nanostructures of meso-(4-cyanophenyl)-substituted Zn(II) porphyrin molecules (*inset* of Fig. 2a) will be described. As substrates, mainly alkali halide single crystals are used, which offer an easy-to-prepare, insulating, and atomically flat surface with well-known properties.

The porphyrin assemblies are formed along step edges and along specific directions of KBr(100) and NaCl(100). Short molecular wires, ringlike structures, long molecular wires ($>250 \text{ nm}$), and oriented multiwires are observed by high-resolution nc-AFM at room temperature. The measured intermolecular distances of $0.5\text{--}0.6$ are similar to natural and biomimetic light-harvesting structures and indicate π - π stacking of the porphyrin rings. The immobilization of the porphyrin molecules is due to electrostatic interaction between the cyanophenyl group and the ionic surface, which yields stable, defect-free molecular aggregates [30, 31]. A similar behavior was also found for porphyrins deposited on thin alkali halide films [47]. In contrast to the parallel orientation of porphyrin molecules deposited on metal surfaces [48], they are tilted on KBr by $35^\circ\text{--}45^\circ$ with respect to the surface. The electrical decoupling as well as the stacking of these porphyrine wires are necessary requirements for the application as light-harvesting structures. Such structures are based on the formation of excitons along the wires and might be used in molecular electronics or machinery. Furthermore, contacting by metal clusters [11, 24, 33], controlled cutting and self-healing processes [32] have been observed and will be summarized.

2.1 Deposition of Porphyrins on Insulating Surfaces

In 2004, Nony et al. [9] showed the confinement of chloro-[subphthalocyaninato] boron-(III) (SubPc) molecules in nanometer-sized pits on KBr(100) which were related to the interaction of the molecular dipole (5.4D) with the electrostatic corrugation of the surface. To enhance the molecule-molecule interaction while still

providing a large molecular dipole moment, a special cyanoporphyrin molecule was synthesized and the chemical structure is shown in the inset of Fig. 2a. The core of the molecule is apolar, while the strong negative polarization of the nitrogen atom induces a dipole moment of 0.36 D allowing to interact with the alternating charges of the ionic surfaces. Porphyrin molecules tend to π - π stack allowing a reasonably strong intermolecular interaction for the stabilization of self-assemblies [30].

Figure 2a shows an nc-AFM image of an electron-irradiated KBr(100) surface [49, 50] at a constant frequency shift of $\Delta f = -20$ Hz, after the evaporation of cyanoporphyrin molecules. The structure of the irradiated pattern is still apparent, and decorated steps are clearly visible. Atomic resolution was obtained on flat terraces, inside the pits, and sometimes also close to the molecular structures [11, 31, 47]. This large-scale topographical image highlights also that only the straight step edges are decorated by porphyrins. As soon as the steps are rounded, the molecular wire becomes interrupted. In Fig. 2b, c, more details about the molecular wire itself are shown. In the lower part of Fig. 2c, an instability is observed where part of the molecular wire is removed, revealing the KBr step underneath it. A model of the molecular arrangement at the ionic step edges reveals the strong intermolecular stacking combined with the electrostatic interaction between the cyanophenyl groups and the alternating ionic potential at the step edges. The two 3,5-di(tert-butyl)phenyl side groups of the molecule are determining the tilting of the wire parallel and perpendicular to the step edge. Along one and two monolayer step edges, single-molecular wires are found, while at higher steps, disordered aggregates of molecules appear [47].

For larger step edges, disordered agglomerates of porphyrin molecules have been observed. Figure 3a shows such agglomerates on a stepped KBr(100) surface which acting as nucleation sites for ordered structures of parallel stacked wires. These multiwires were found to be mainly oriented along the [110]-direction of the KBr substrate. The number of parallel stacked wires can be controlled by the deposition rate. Assemblies with sizes from a few parallel wires up to several hundred nanometer wide structures are possible [31]. Figure 3b shows a high-resolution nc-AFM image of such parallel molecular wires separated by 2.4 ± 0.2 nm. This separation corresponds to approximately five lattice spacings of the substrate. In a work of Pšenčík et al. [51], distances between different bacteriochlorophyll stacks in natural chromosomes of 2.1–3.0 nm have been determined which is in the same order of magnitude as observed by Maier et al. for the porphyrin assemblies. However, unlike at the step edges in [100]-direction, the intermolecular distance (0.56 ± 0.01) within a wire differs from the KBr lattice spacing of 0.47 between two K^+ ions along the [110]-direction. This indicates that the dimensions of the molecule require a larger separation than the K^+ intervals provide. However, the partially negative-charged cyanophenyl groups are forced into position by the alternating K^+ and Br^- ions along the step edges in [100]-direction.

In [110]-direction, a positive potential well is formed by the potassium ions which are not interrupted by bromide ions. This allows the cyanoporphyrins to adjust to their thermodynamically preferred intermolecular spacing while stabilizing

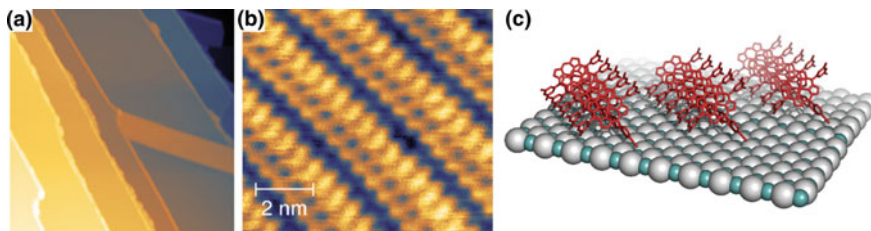


Fig. 3 **a** nc-AFM topographical overview of atomic KBr step edges decorated with porphyrin molecules and a molecular carpeted (multiwire) in $[110]$ substrate direction. **b** Intramolecular resolution of such a wire and parallel rows of the stacked molecules are visible. **c** Schematic model of the molecular multiwire on KBr [31]

in the positive potential well along the K^+ ions by the partial negative charge of the cyano end groups. Figure 3c shows the proposed multiwire arrangement in $[110]$ -direction taking into account the steric hindrance of the side groups and the measured intermolecular distances. Compared to the wires at the step edges, the angle between the porphyrin cores and the wire axis of the multiwires is enlarged to (43° – 45°). It was concluded that the multiwires are attached by the cyanophenyl groups pointing downwards to the surface and the bulky side groups standing out on one side as depicted by the asymmetric shape of the molecule in the high-resolution image (Fig. 3b). Depending on the tilt angle of the stacks, monolayer heights between 1.5 and 2.0 nm were measured.

We showed further that the direction of the wires can be controlled by the atomic structure of the substrate so that complex molecular assemblies can be formed. NaCl is chemically and physically similar to KBr and is therefore an interesting sample to investigate the influence of the lattice distance of the substrate to the molecular self-assemblies. The lattice constant of NaCl is 5.65 Å which is very close to the spacing of 5.6 Å between the stacked molecules. An overview nc-AFM topography image of the molecular assemblies on NaCl(100) is shown in Fig. 4a. The step edges show no ordered molecular decorations and have no specific direction; however, single-wire decoration as on the KBr(100) has been found along steps in $[100]$ -direction. Furthermore, a large amount of multiwires growing across the terraces from kink sites at step edges was observed. A major difference between the self-assemblies on KBr and NaCl is the formation of crossing molecular carpets or networks of molecular wires which is shown in Fig. 4a. The observed angles between the wires are 90° and 45° indicating a growth-oriented in all major crystallographic surface directions. The shape and thickness of the molecular structures do not differ along the $\langle 100 \rangle$ and $\langle 110 \rangle$ directions. The intermolecular distance of 5.65 Å making the wires along the $\langle 100 \rangle$ directions on NaCl more favorable compared to KBr and the molecules is most certainly adsorbed at every sodium atom. Furthermore, wires along the $\langle 110 \rangle$ directions can still grow from kink sites or wire junctions, which is depicted in Fig. 4b, c for the structural models of KBr(001) and for NaCl(001).

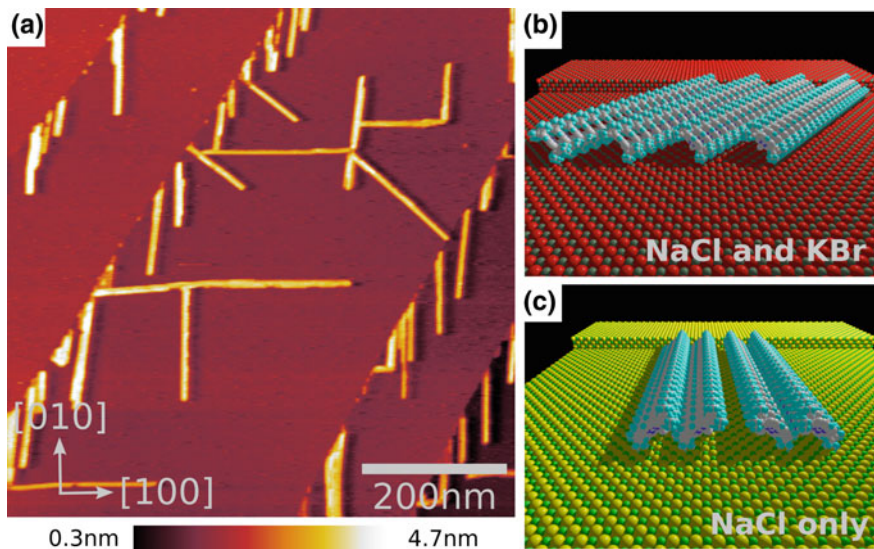


Fig. 4 **a** nc-AFM topography of the cyanoporphyrin molecular wires on NaCl. The molecular wires are oriented along the [100]- and [110]-directions. Schematic views are depicted in **b** and **c** [47]

2.2 Contacting Porphyrin Structures

The previous section showed the possibility to form and control the growth direction of molecular wires along step edges and across terraces. A requirement in molecular electronics is the contacting of such molecular structures with metal contacts. Evaporated gold forms small clusters on KBr and NaCl with a visible diameter of 2–10 nm and a height of roughly 1.5 nm. Figure 5a shows a measurement of such Au clusters and molecular assemblies of porphyrin wires [24]. The zoomed area in (b) highlights one wire contacted at both ends by a gold cluster. The LCPD [26] image in Fig. 5c resolves differences among the KBr surface, the Au nanoclusters, and the molecular wire. Between the KBr surface and the Au nanoclusters, differences of ≈ 250 mV and between Au nanocluster and the molecular wire of ≈ 220 mV were measured. The local dipole moment of the molecules defines the LCPD values at the wire which was measured to be $\Delta V_{\text{LCPD}} = 180 \pm 20$ mV.

The LCPD can be related to the difference in dipole moment densities (Δp) by $\Delta V_{\text{LCPD}} = 1/\epsilon_0 \Delta p$ which results in 0.5 D nm^2 . Taking a molecule density of 0.72 nm^{-2} [31] results in an average dipole moment density difference per molecule of 0.36 D. This is a reasonable value in comparison with the absolute dipole moment of a single porphyrin of 4.37 D. However, the well-known averaging effect [52] in KPFM measurements at very close proximity to the surface (<1 nm) has to

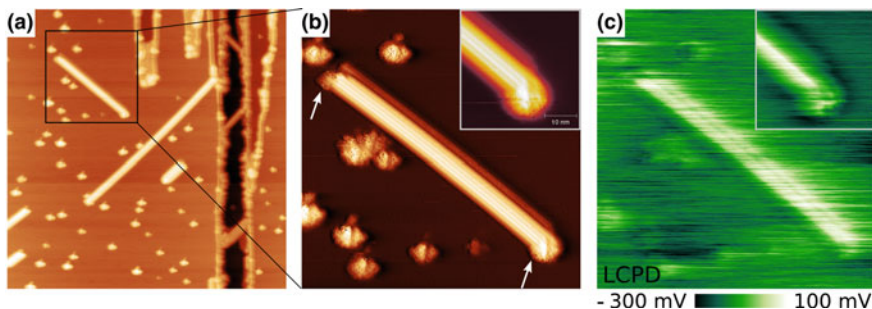


Fig. 5 nc-AFM measurements of porphyrin multiwires on Au-decorated KBr(100). **a** shows a $300 \times 300 \text{ nm}^2$ scan with various wires along the [110]-direction. **b** Topography and **c** LCPD measurements give a closer look of the region ($100 \times 100 \text{ nm}^2$) marked by a black frame in **a**. A porphyrin multiwire assembly is formed between two Au clusters marked in **b**. The insets ($30 \times 30 \text{ nm}^2$) highlight details of the lower end of the wire [24]

be considered and the absolute values can be assumed to be a lower limit for the dipole moment.

Even so the molecular structures can be contacted by metal clusters, an electrical readout is still not possible. The goal of the next study was therefore the electrical contacting of such molecular porphyrin wires. For that purpose, electrodes using nanostencil lithography (NL) were fabricated, which circumvents the use of resist layers and etching steps [53]. Building up the molecular wires and metal electrodes on a crystalline insulating layer required a complex sample fabrication, involving several evaporation and annealing steps. The starting point was an n-doped (001)-oriented GaAs wafer for subsequent use as a conductive substrate for the electrodes. A NaCl layer having a thickness of approximately 2.5 nm (sufficient for efficiently suppressing electron tunneling) was evaporated through a stencil mask. The porphyrin molecules and some Au cluster were evaporated onto the entire sample. Metal electrodes were fabricated by using the same mask as used for NaCl evaporation, but with a lateral offset. This produced a metal pad that partly overlapped with the NaCl pad. Electrical contact of the metal pad was established to the GaAs substrate in the region without overlap with the NaCl layer. As electrode material Cr was used, diffusion effects could be strongly minimized compared to Au electrodes. To facilitate the contacting of molecular wires, dendritic apertures were cut into the edge of the stencil membrane to form structured metal electrodes on the NaCl layer (cp. Fig. 6a) [33].

Figure 6a, b shows the topography and the contact potential difference (CPD) around an area near an electrode structure of such a sample, respectively. A measurement with increased resolution of a porphyrin multiwire contacted on one side by an Au cluster and on the other to the Cr electrode is shown in Fig. 6c. The wire was approximately 100 nm long with a height of 1 nm. This multiwire was built up from several individual molecular wires, as we deduced above, cp. Fig. 3. Taking the width of approximately 10 nm into account, the multiwire consisted of 4–5

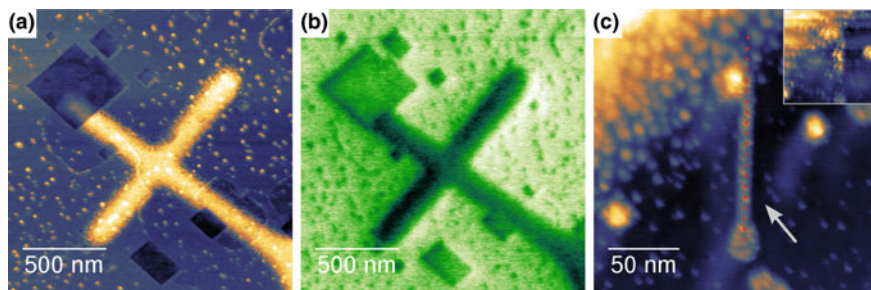


Fig. 6 **a** Cr electrodes are evaporated after the molecular wires on top of a NaCl thin film on a GaAs substrate. The molecules were evaporated first, then the sample was annealed to 480 to induce the formation of molecular wires, and finally, Cr electrodes were evaporated. **b** shows the simultaneously acquired CPD image highlighting the different materials ($\Delta\text{CPD} = 720$ mV). Molecular wires were also found near the electrodes as highlighted by an *arrow* in **c**. Bias spectroscopy was performed along the red dotted line, however the wire was destroyed afterward, see inset image [33]

single-molecular wires. To test the conductivity distance, spectroscopy measurements along the structure have been performed using the tip as the second electrode. At each measurement point (red dots along the wire in Fig. 6c), the tip was moved 23.5 nm toward the surface, measuring frequency shift, amplitude, dissipation, and current values. A sample bias voltage of $V_{\text{bias}} = 2.5$ V was applied. Above the Cr electrode, a current of up to 40 pA was measured, whereas above the molecular wire, no current could be detected. However, the molecular structure was completely damaged after the measurement (inset of Fig. 6c) most probably due to entering the repulsive regime of the interaction forces during the spectroscopic measurements. The measured onset of the current above the Cr electrode indicates that the electrode was connected successfully via the GaAs sample and also that such conductance measurements are in principle feasible.

2.3 Cutting and Regeneration of Porphyrin Structures

Already in the first measurement of porphyrin wires, it was observed that the structures can be easily destroyed by the AFM tip (cp. Fig. 2c). Figure 7 shows a series of topographical measurements of an intentionally deformed porphyrin multiwire obtained by nc-AFM at room temperature with an amplitude of 5.0 nm at a frequency shift of -5.1 Hz. In order to avoid accidental tip-induced modifications, the surface was scanned at a relatively large tip-sample distance ($\gamma = -0.5$ fN $\sqrt{\text{m}}$). After Fig. 7a was obtained, the wire was cut by deactivating the tip-sample distance controller eleven times at the indicated positions. The multiwire was divided into three parts but surprisingly, in the next measurement, shown in Fig. 7c, the wire grew, and the gap between the middle and upper parts

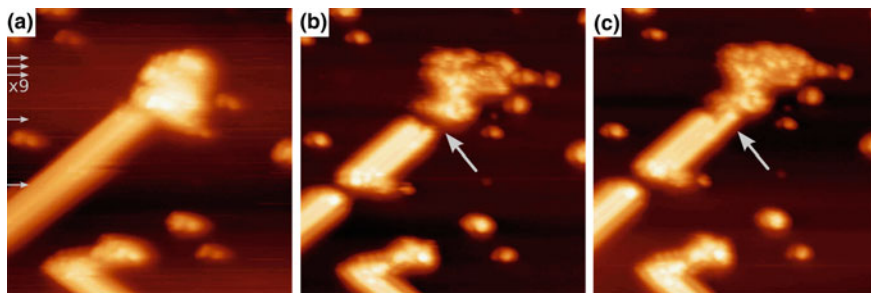


Fig. 7 Intentional deformations of a porphyrin multiwire connected to an Au cluster ($90 \times 90 \text{ nm}^2$). **a** Before cutting with the AFM tip, **b** with two distinct cuts, and **c** self-healing at room temperature [32]

became smaller, indicated with an arrow. Since no significant instability of the cantilever oscillation was observed, the regeneration process seems not be related to tip-induced modifications (i.e., deposition of molecules from the tip covered by molecules). It is most likely that mobile molecules, existing on the KBr(100) surface, self-assembled to close the gap in the wire. This behavior might be very important to achieve highly robust and self-healing future molecular devices.

3 Mechanical Properties

A general strategy allowing immobilization of single molecules on an insulating substrate at room temperature is a prerequisite for molecular electronics. In Sect. 2 the self-assembly and the stabilization of porphyrin molecules was presented. The stabilization at room temperature occurred due to π - π interaction between the cores of the molecules, while the substrate interaction controlled the absorption of the assemblies on ionic surfaces [47]. To allow an even stronger molecule surface interaction, stronger localized and directed dipole moments are necessary. Custom-designed syn-5,10,15-tris(4-cyanophenylmethyl)truxenes (inset of Fig. 8a) contain three flexible cyanobenzyl groups, possessing a large dipole moment, which immobilizes even single molecules at specific sites of the ionic substrate allowing them to be imaged by nc-AFM at room temperature [34].

Figure 8b shows molecular dynamics (MD) calculations of the truxene molecule attached to a kink of a KBr step edge. The combination of the three flexible binding groups interacting independently with the surface is crucial for anchoring and enhances the binding energy at the kinks, while the molecules at the bare step edges are at room temperature still mobile, leading to the fuzzy contrast in Fig. 8a. The molecule-substrate interaction was even found to be large enough to restructure the ionic surface providing anchoring sites for the single molecules. Figure 8c shows a former rectangular KBr pit which was reconstructed while evaporating the truxene

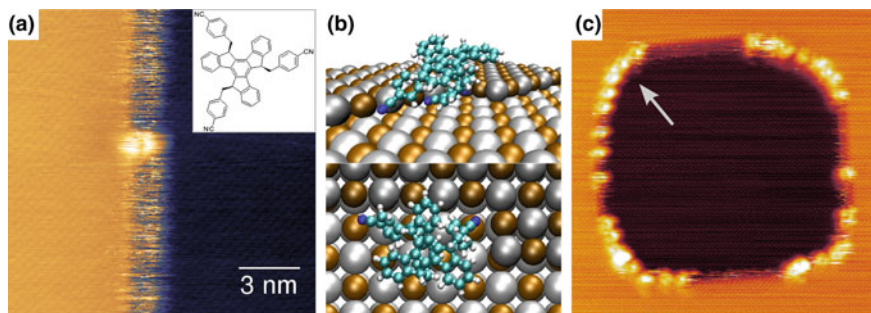


Fig. 8 **a** Single truxene molecule (*inset*) stabilized at a kink of a KBr step edge. The fuzzy contrast at the atomic step edge is induced by mobile molecules [34]. **b** MD calculations confirm the attachment of the cyanobenzol groups to the kinks and the overall stabilization of the molecule. **c** During deposition of the molecules, the surface of KBr is adopted to provide sufficient adsorption sites for the molecules. Former rectangular pits are transformed to round-shaped structures [35]

molecules to the surface [35]. So the mechanical properties such as elasticity and mobility of molecules on the surfaces are crucial physical parameters to understand, control and predict molecular self-assemblies for applications.

3.1 Elasticity of Single Molecules

Recently, atomic force microscopy has made remarkable progress in imaging organic molecules allowing inner structure observations within molecules [15]. Although the atoms and bonds of flat molecules have been resolved, the study of three-dimensional molecules such as C_{60} and the measurement of intrinsic mechanical properties at the atomic level within a molecule is still challenging. We presented submolecular resolution of the C_{60} molecule obtained by combined nc-AFM and STM in 2011 revealing its chemical structure, describing unambiguously the C_{60} orientations on the substrate as well as local elasticity measurements. The same molecule was used by Gross and co-workers [54] to discriminate the bond order of individual carbon–carbon bonds in polycyclic aromatic hydrocarbons and fullerenes. Moreover, three-dimensional spectroscopic measurements of the interaction force and the tunneling current above single molecules allowed us to obtain a detailed insight in the observed contrast. By our technique, we could show site-specific stiffnesses within the molecular structure which are related to the local elastic properties of the fullerene structure and confirms its predicted robustness at the atomic scale which is not possible by STM alone. Recently, the molecular stiffness of a single CO molecule was determined with a similar setup [55].

Systematic three-dimensional (3D) spectroscopic nc-AFM measurements at 77 on C_{60} molecules being adsorbed on top of self-assembled C_{60} islands have been

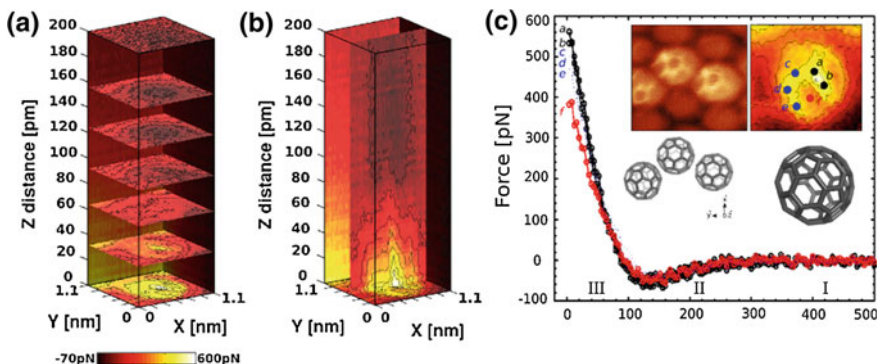


Fig. 9 **a** 3D force field $F_z(x, y)$ acquired by nc-AFM at different tip-sample separations and **b** $F_z(x, z)$ cross section taken at the center of the molecule, revealing the contrast evolution with respect to the tip-molecule distance z . Parameters, $1.1 \times 1.1 \times 0.5 \text{ nm}^3$ with $60 \times 60 \times 128$ data points, $V_{\text{tip}} = 300 \text{ } \mu\text{V}$, $A = 60 \text{ pm}$ [37, 40]

performed [37]. Figure 9a, b illustrate the evolution of the 3D force field above a single molecule $F_z(x, y)$ at different tip-sample distances as well as a vertical cross sections $F_z(x, z)$ taken at the center of the molecule, respectively. For tip-sample distances smaller than 200 pm, the detected contrast appears as a homogeneous dark protrusion above the C_{60} and is induced by attractive forces of up to -70 pN . Simultaneously, small tunneling currents of 10–20 pA have been detected. For tip-sample distances smaller than 100, the observed contrast in the $F_z(x, y)$ field shows a local increase up to positive values with submolecular resolution. This shows that a variation of the tip-sample distance of only 100 pm is sufficient to induce the disappearance of the inner molecular structure during imaging. The inset of Fig. 9c presents the constant-height force map of the closest tip-sample distance, which reveals the chemical structure of the C_{60} with an edge between polygons on top of the molecule. The deduced orientation of the C_{60} is just plotted below [37, 40].

The analysis of individual force curves is shown in Fig. 9c. Specific sites (see right inset of Fig. 9c) corresponding to carbon sites (marked a–e) and the center of a carbon ring (f) were analyzed. In region I and II, more far away from the surface, the curves are nearly indistinguishable as expected for long-range attractive forces. For tip-sample distances smaller than 100 pm (region III), differences induced by the repulsive force regime have been observed. While the total interaction force obtained in positions a and b reaches a maximal value of 550–570 pN, the value is slightly lowered to about 460–500 pN due to a slightly larger tip-sample distance for similar carbon sites c, d, and e. Finally, the center of the carbon ring (site f) exhibits the smallest repulsive force of 390 pN.

The slopes of the force-distance curves in the repulsive force regime can be interpreted as the local elastic properties appearing between the structure of the C_{60} molecule and the Cu-terminated tip. Above carbon atoms (sites a–e), this vertical

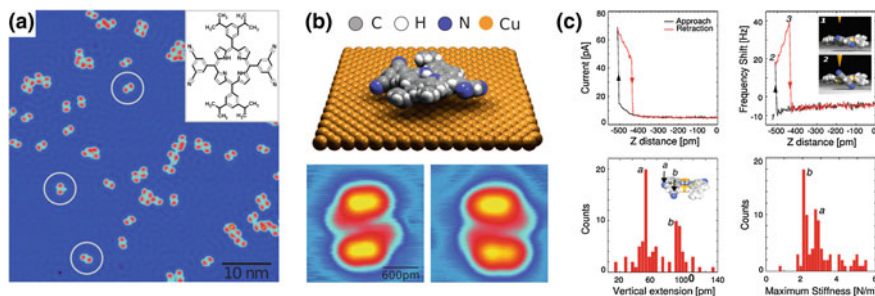


Fig. 10 **a** STM topography in constant current mode of H₂TBCPP on Cu(111) showing individually adsorbed porphyrin molecules oriented along three directions of the substrate (circles). **b** Schematic view of the saddle conformation and STM images of the two enantiomers [56]. **c** Individual approach–retract curves taken above a single nitrogen atom and the determined vertical extension as well as the tip–sample stiffness during the switching process [39]

force gradient is found to be 7–9 N/m, whereas above the center of the carbon ring (site f), this value is lowered to 4 N/m. Since only a minor dissipation contrast was detected, revealing a pure elastic interaction as well as a stiffer tip apex was assumed, the observed site-dependent force variations have been related to submolecular stiffness variations of the C₆₀ structure.

Another example of the local deformation of a single molecule on a surface is the study presented by Pawlak et al. [39]. H₂TBCPP porphyrin molecules (chemical structure in inset of Fig. 10a) were thermally evaporated on a cold Cu(111) substrate ($T = -190$ K). Figure 10a shows individually adsorbed molecules oriented along the [110]-direction or an equivalent symmetry direction (marked by circles). The di-tert-butylphenyl groups of each molecule appear as bright protrusion, while the di-cyanophenyl groups are darker which is described also for similar molecules as saddle conformation (cp. Fig. 10b upper image) [57]. The two di-cyanophenyl groups are slightly rotated compared to the molecular center leaving one carbonitrile group closer to the Cu(111) substrate than the other and resulting in two enantiomers as shown in the lower part of Fig. 10b.

The submolecular elastic properties of this molecule have been studied again by combined 3D force and tunneling spectroscopy at low temperatures ($T = 4.8$ K). The frequency shift data set revealed four distinct submolecular regions at the periphery of the molecule with a strong positive frequency shift, the rest of the values is negative hence still in the attractive force regime. These points can be related to the carbonitrile groups of the porphyrin molecule. The forward and backward data sets revealed a strong hysteresis in these areas (transition 1–2). The same phenomenon is visible in the tunneling current channel, showing an abrupt jump to higher currents. The corresponding distance-dependent Δf and I_t curves are shown in the upper panel of Fig. 10c. Both curves clearly indicate a hysteresis loop at the point of closest tip–sample distance between the forward and backward scan, while further away they match perfectly. Therefore, tip changes can be excluded as well as a strong influence by repulsive forces.

The oscillation amplitude used in this studies was $A = 40\text{--}60$ pm and the hysteretic behavior was attributed to the formation of a junction between the Cu-terminated tip and the N atom of the targeted carbonitrile group. Upon retraction, the bond formation is strong enough to lift the carbonitrile group (transition 2–3). Within this region, the tunneling current slightly decreases, because the carbonitrile group is disconnected from the surface and lifted up. At the same time, the frequency shift increases in a discontinuous manner, suggesting a strong tip–molecule interaction. The jump back to the initial curve shape (point 3) indicates that the molecule recovers its initial state in the saddle conformation. The vertical lifting process happens independently of the targeted carbonitrile group and is fully reversible.

To extract the local stiffness k_{ts} of this submolecular contact, the length of the hysteresis loop (z -distance between point 2 and 3) as well as the maximum frequency shift were determined in a statistical analysis. The vertical extension as well as the stiffness is plotted in the lower diagrams of Fig. 10c. Both histograms have two pronounced peaks (a and b) attributed to two different lifting processes, one for a carbonitrile group which initially have been more far away from or closer to the surface, respectively. The maximum stiffness determined for these two distinct contacts is $k_{ts(a)} = 2.9$ N/m and $k_{ts(b)} = 2.0$ N/m.

3.2 Manipulation of Single Molecules

Directed molecular manipulation is a key step toward the understanding of molecular electronics as well as to build up single-molecular devices. To initiate and control molecular motion on a surface mechanical, chemical, or electrical interactions are used. However, as was described in Sect. 3.1, elasticity of molecular structures plays a major role in all diffusion processes. In response to the just above discussed local tip–sample force, the molecular structure is elastically deformed and leads finally also to a controlled rotation [37, 39].

If the tip is approached slightly further (20 are sufficient!) compared to the separations that induce only an elastic deformation, the bond between the carbonitrile group and the Cu tip apex is sufficiently strong to induce a rotation of the molecule by 60° . However, the exact lateral position of the tip is important for the strength of the interaction and the bond might already not be strong enough anymore to induce the rotation. The target area for a clockwise rotation is highlighted by the red area in Fig. 11a. The rotation direction depends on the targeted carbonitrile group, for a clockwise rotation the red areas, while for an anticlockwise direction the green areas have to be approached by the tip. An example of both rotation directions is shown in the overview images in Fig. 11b. For all adsorption directions and enantiomers, this behavior was found to be valid success rate of 75 % [39].

Some details about this manipulation process can be gained by analyzing the respective distance-dependent measurements as presented in Fig. 11c. The tunneling current plotted in the upper diagram shows again the discussed

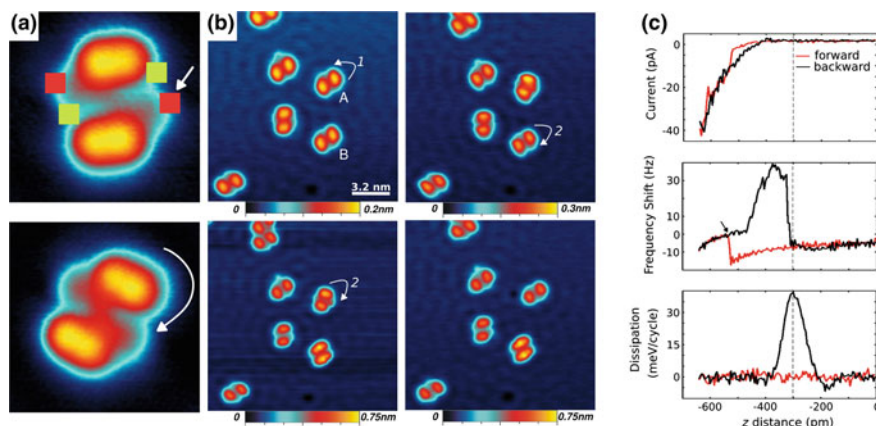


Fig. 11 **a** STM images showing a single rotation of a H2TBCPP molecule on Cu(111), the white arrow shows the used position of the z spectroscopic curve for the clockwise rotation (red areas). Counterclockwise rotations can be induced at green areas. **b** Images of successive manipulation processes. **c** Typical distance-dependent curves of the tunneling current, the frequency shift, and the dissipation leading to a molecular rotation [39]

abrupt jump when contacting tip and molecule. However, the hysteresis is strongly distorted due to the rotation. For the frequency shift and the dissipation, significant features are visible in the retraction curves. The hysteresis in the frequency shift channel is extended, while the dissipation rises up to values of ≈ 40 meV/cycle. This peak in the backward dissipation signal is one of the main characteristics of a successful and force-induced rotation process. Similar to the elastic deformation, a junction is formed between the tip apex and the molecule upon approach. During retraction, first the di-cyanophenyl group is lifted up; however, the bond is stronger and the group is lifted up further. Upon this process, the second carbonitrile group is partly detached from the surface and laterally moved to a neighboring equivalent adsorption site. This detachment gives rise to stochastic changes of the tip-sample interaction and therefore to an increase of the frequency shift and the dissipation. Upon retraction of the tip and breaking of the tip-carbonitrile bond, the molecule relaxes to the new equilibrium position.

Another important manipulation process is a lateral manipulation of molecular structures for understanding their mechanical properties. The most fundamental and clean approach to understand these properties is a single-molecular wire pulled off a surface measured with atomic-scale resolution. Just recently, Kawai et al. [21] presented a study of the mechanical behavior of in situ polymerized fluorene wires with a length of 10–100 by pulling individual wires with a tip of a low-temperature nc-AFM. Figure 12a shows an Au(111) surface covered by molecular wires deposited by polymerization of a dibromoterfluorene (DBTF) precursor, schematically presented in the lower part of Fig. 12b [58]. The chemical structure and a high-resolution image of one end of the wire is shown in the inset. Most of the wires are physisorbed along the fcc stripes of the Au(111) herringbone structure at 4.8.

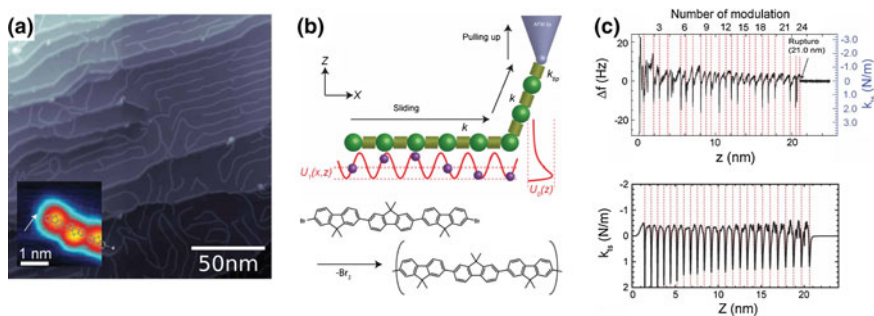


Fig. 12 **a** Constant current STM measurement of the polymerized DBTF molecules to polyfluorene chains on an Au(111). The *inset* shows a zoom-in STM image near one end of a molecular chain. A schematic drawing of a physical model while pulling up the molecular chain as well as the DBTF molecule during the polymerization process is shown in **b**. **c** Experimental frequency shift data measured while retracting the tip after contacting and pulling a chain and calculated force gradient [21]

By contacting the AFM tip to one end of the wire and pulling it up, the frequency shift at the resonance of the tuning fork sensor was recorded (Fig. 12c). The measured periodic variations of the force gradients correspond to the step-by-step detachment of fluorene units as shown by the schematic model in Fig. 12b. Calculations based on an extended Frenkel–Kontorova model reproduced the measured mechanical behavior and revealed that the stick forces and energy barriers are almost independent of the unit being detached.

All the presented examples demonstrate that the mechanical behavior of single molecules as well as low-dimensional molecular assemblies on surfaces can be characterized with atomic-scale precision in a control manner by high-resolution nc-AFM measurements.

4 Electrical Properties of Single Molecules

Also the electronic properties of single-molecular adsorbates play a decisive role in many fundamental processes as for instance in catalysis [59, 60], organic photovoltaics [61], and particularly also in molecular electronics. The adaptation of the energy alignment and local charging processes significantly modify the electronic structure of both the molecule and substrate. Combined nc-AFM and STM offers not only to image the topographical structure down to the atomic scale and measure, and manipulate mechanical properties as shown in the sections before, but also to determine local electronic properties such as the local work function or charge density. One of the major advanced microscopy techniques allowing to determine such properties is called KPFM [62]. In this section, we will just briefly introduce

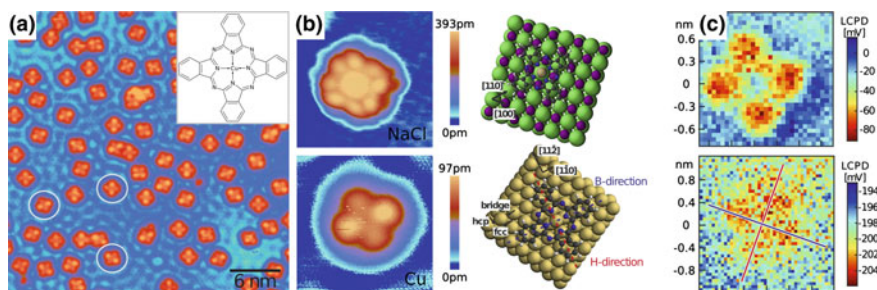


Fig. 13 **a** STM constant current image of CuPc molecules (*inset*) on Cu(111), three different orientations have been observed. **b** High-resolution constant current images and DFT-calculated adsorption geometries of CuPc on 2ML NaCl on Cu(111) (*top*) and bare Cu(111) (*bottom*). **c** LCPD showing intramolecular resolution of both configurations obtained by bias spectroscopy [63]

some recent studies focusing on submolecular resolution allowing to determine intramolecular charge densities.

Figure 13 shows the structure and local electronic properties of copper phthalocyanine (CuPc) molecules [*inset* of (a)] adsorbed on a metallic Cu(111) substrate, either directly, or on top of a decoupling NaCl bilayer [56, 63]. A comparison of these strongly and weakly interacting systems allows to directly conclude on structural distortions and charge distributions within the single molecules. While CuPc exhibits a fourfold D_{4h} symmetry in the gas phase, it is reduced to twofold D_{2h} symmetry by the adsorption on the metal surface, resulting in three different orientations on the Cu(111) substrate. For metal phthalocyanine molecules, it is assumed that an electron transfer from the metal surface to the molecule takes place [64, 65]. For CuPc on Cu(111), the overall charge transfer is assumed to be two electrons [66, 67]. However, in the presence of a NaCl bilayer, this charge transfer is affected and the electronic structure of the molecule remains nearly as in its gas phase [7].

In Fig. 13b, constant tunneling current images and DFT simulations of a single CuPc molecule adsorbed on a 2ML NaCl on Cu(111) (*top*) and bare Cu(111) (*bottom*) are shown. The fourfold symmetry for the molecule on the NaCl bilayer is as expected preserved indicating rather weak molecule–surface interactions. The DFT-calculated adsorption geometry in the lowest energy configuration reveals that in the energetically most favorable conformation, the central Cu atom is placed above a Cl^- ion. Due to the coinciding fourfold symmetry of the NaCl layer and the molecule, all four benzopyrrole rings are located at equal adsorption sites. The reduced twofold symmetry, one pair of opposing benzo-pyrrole rings appears brighter than the other, of the CuPc molecule on the bare Cu(111) surface is clearly visible in the measurement below. The combination of the sixfold symmetry of the Cu(111) and the fourfold symmetries of the molecule resulting in a twofold symmetry of the combined system which is also visible in the DFT calculations.

To determine the local electrostatic potential and the distribution of charge inside these two setups, 3D local bias spectroscopy measurements have been performed. The mapping of the LCPD as a function of the lateral position above the surface at constant height allows to obtain subnanometer scale LCPD values which can directly be connected with the local dipole moments induced by the local electric field between tip and molecule/surface. Figure 13c shows the LCPD of both setups the one on the NaCl bilayer again in the upper row. The contrast above the molecule is shifted to lower LCPD values compared to the substrate, and the overall maximal shift is ≈ 80 mV for the molecule on the NaCl and only ≈ 10 mV on the bare Cu(111). However, the central Cu atom of the CuPc appears at more positive LCPD values than the benzopyrrole rings. The major difference of the CuPc adsorbed on Cu(111) beside the overall lower contrast is the completely broken symmetry in between the benzopyrrole rings. While the two rings along the red line feature similar contrast, one of the rings along the blue line features brighter contrast than the other.

A more negative LCPD value corresponds in the used setup to a more negative charge at the surface, here the benzopyrrole rings. For the CuPc on the NaCl layer, the charge distribution between the center Cu atom and the four benzopyrrole rings seems to be preserved, while the surface–molecule interaction in the case of the Cu(111) sample reduces this charge contrast by a different adsorption geometry but also by a charge transfer between them. The asymmetry within the LCPD contrast for CuPc on Cu(111) could also be proven by DFT calculations and is based on the fact that one benzopyrrole ring adsorbs above a fcc—while the other one above a hcp—hollow site. This gives rise to different molecule–substrate interactions at the two positions, and hence to different charge densities.

Another study was performed on a functionalized phenylethynylbenzene molecule (FFPB) providing an electron-donating and electron-accepting group (see inset in Fig. 14) [42]. The molecule was self-assembled on an Au(110)-(1 \times 2)

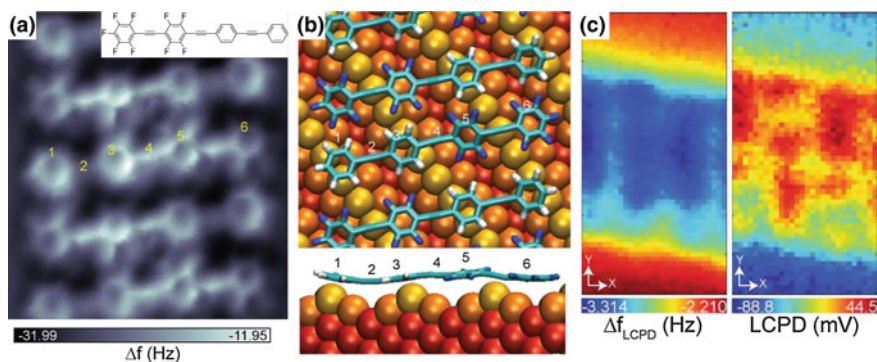


Fig. 14 **a** Frequency shift image of a donor–acceptor molecule (FFPB, *inset* chemical structure) self-assembled on Au(110)-(1 \times 2). **b** Side and top views of the relaxed molecule on the Au substrate using DFT. **c** A 3D bias voltage-dependent measurement revealed the frequency shift and the LCPD measured with an Au tip [42]

surface forming one-dimensional supramolecular structures. Figure 14a shows the complex chemical structure in the frequency shift image revealed by atomic force microscopy. It was observed that a major stability requirement of these self-assemblies is the formation of directional hydrogen bonds. A comparison of detailed geometrical deformations of the molecule on the substrate with density functional calculations is in perfect agreement with the measurements (cp. Fig. 14b). Furthermore, detailed bias spectroscopy measurements have been carried out providing the intramolecular charge distribution and allowed to identify the fluoro-substitution sites of each molecule. The data have been acquired by fitting the measured bias spectroscopy data to a parabola and calculating the LCPD and the corresponding frequency shift as shown in Fig. 14c. The LCPD contrast is governed by the local dipole and charge state, and the strongly electronegative fluorine atoms induce stronger local dipoles than the CH bonds. Therefore, the direction of each molecule could unambiguously be determined. However, the dipole of this molecule is located mainly parallel to the surface and the variations only appear due to the geometrical distortions and are influenced by the substrate interaction.

5 Summary

The presented results show that scanning probe microscopy techniques serve as unique investigation tools concerning fundamental questions related to molecules on surfaces. The deposition of molecules on insulating surfaces was demonstrated, and the in-detail characterization of the mechanical properties revealed a clear picture of the adsorption and stabilization process. Molecules with functionalized groups have been sensitized and allow together with an appropriate substrate the controlled growth of single molecules and various assemblies. The electrical characterization at the molecular scale is still in progress and a very active research field. However, the presented results already allow to determine intramolecular charge transfer processes and might also lead to the development of new functional molecules. Future studies include the simultaneous excitation by visible light to study also optically induced charge transfer processes within single molecules.

Acknowledgments The contributions from S. Maier, L. Zimmerli, S. Freymy, L. Gross, R. Pawlak, B. Such and S. Kawai are highly appreciated. Such research would not be possible without the interdisciplinary collaborations between chemists and physicists; therefore, many thanks to F. Diederich, A. Echavarrén, S. Decurtins, Ch. Housecroft, and E. Constable as well as the involved students. Many thanks also to E. Meyer and A. Baratoff for the continuous support and stimulating discussions. The work reported in this chapter was financially supported by the Swiss Nanoscience Institute, the Swiss National Science Foundation, the Joint Swiss-Polish Research Programme PSPB-085/2010, and the Commission for Technology and Innovation CTI.

References

1. Mirkin, C.A., Ratner, M.A.: Molecular electronics. *Annu. Rev. Phys. Chem.* **43**(1), 719–754 (1992)
2. Weibel, N., Grunder, S., Mayor, M.: Functional molecules in electronic circuits. *Org. Biomol. Chem.* **5**, 2343–2353 (2007)
3. Heath, J.R.: Molecular electronics. *Annu. Rev. Mater. Res.* **39**(1), 1–23 (2009)
4. Binnig, G., Rohrer, H., Gerber, C., Weibel, E.: Surface studies by scanning tunneling microscopy. *Phys. Rev. Lett.* **49**(1), 57 (1982)
5. Binnig, G., Rohrer, H., Gerber, C., Weibel, E.: Tunneling through a controllable vacuum gap. *Appl. Phys. Lett.* **40**(2), 178 (1982)
6. Binnig, G., Rohrer, H.: Scanning tunneling microscopy. *Helv. Phys. Acta* **55**(6), 726–735 (1982)
7. Repp, J., Meyer, G., Stojkovic, S., Gourdon, A., Joachim, C.: Molecules on insulating films: Scanning-tunneling microscopy imaging of individual molecular orbitals. *Phys. Rev. Lett.* **94**, 026803 (2005)
8. Binnig, G., Quate, C., Gerber, C.: Atomic force microscopy. *Phys. Rev. Lett.* **56**(9), 930 (1986)
9. Nony, L., Gnecco, E., Baratoff, A., Alkauskas, A., Bennewitz, R., Pfeiffer, O., Maier, S., Wetzel, A., Meyer, E., Gerber, C.: Observation of individual molecules trapped on a nanostructured insulator. *Nano Lett.* **4**(11), 2185–2189 (2004)
10. Fendrich, M., Kunstmann, T., Paulkowski, D., Moller, R.: Molecular resolution in dynamic force microscopy: topography and dissipation for weakly interacting systems. *Nanotechnology* **18**(8), 084004 (2007)
11. Glatzel, T., Zimmerli, L., Meyer, E.: Molecular assemblies on insulating ultrathin films analyzed by nc-AFM and KPFM. *Isr. J. Chem.* **48**(2), 107 (2008)
12. Milde, P., Zerweck, U., Eng, L.M., Abel, M., Giovanelli, L., Nony, L., Mossoyan, M., Porte, L., Loppacher, C.: Interface dipole formation of different ZnPcCl₈ phases on Ag(111) observed by Kelvin probe force microscopy. *Nanotechnology* **19**(30), 305501 (2008)
13. Gross, L., Mohn, F., Moll, N., Liljeroth, P., Meyer, G.: The chemical structure of a molecule resolved by atomic force microscopy. *Science* **325**(5944), 1110 (2009)
14. Schütte, J., Bechstein, R., Rahe, P., Langhals, H., Rohlfing, M., Kühnle, A.: Single-molecule switching with non-contact atomic force microscopy. *Nanotechnology* **22**(24), 245701 (2011)
15. Gross, L.: Recent advances in submolecular resolution with scanning probe microscopy. *Nat Chem* **3**(4), 273–278 (2011)
16. Hauptmann, N., Mohn, F., Gross, L., Meyer, G., Frederiksen, T., Berndt, R.: Force and conductance during contact formation to a C₆₀ molecule. *New J. Phys.* **14**(7), 073032 (2012)
17. Morita, S., Yi, I., Sugimoto, Y., Oyabu, N., Nishi, R., Custance, O., Abe, M.: Mechanical distinction and manipulation of atoms based on noncontact atomic force microscopy. *Appl. Surf. Sci.* **241**(1–2), 2–8 (2005)
18. Sugimoto, Y., Pou, P., Custance, O., Jelinek, P., Abe, M., Perez, R., Morita, S.: Complex patterning by vertical interchange atom manipulation using atomic force microscopy. *Science* **322**(5900), 413–417 (2008)
19. Loske, F., Kühnle, A.: Manipulation of C₆₀ islands on the rutile TiO₂(110) surface using noncontact atomic force microscopy. *Appl. Phys. Lett.* **95**(4), 043110 (2009)
20. Wagner, C., Fournier, N., Tautz, F.S., Temirov, R.: Measurement of the binding energies of the organic-metal perylene-teracarboxylic-dianhydride/Au(111) bonds by molecular manipulation using an atomic force microscope. *Phys. Rev. Lett.* **109**, 076102 (2012)
21. Kawai, S., Koch, M., Gnecco, E., Sadeghi, A., Pawlak, R., Glatzel, T., Schwarz, J., Goedecker, S., Hecht, S., Baratoff, A., Grill, L., Meyer, E.: Proceedings of the National Academy of Sciences (2014)
22. Gross, L., Mohn, F., Liljeroth, P., Repp, J., Giessibl, F.J., Meyer, G.: Measuring the charge state of an adatom with noncontact atomic force microscopy. *Science* **324**(5933), 1428–1431 (2009)

23. Kitamura, S., Suzuki, K., Iwatsuki, M., Mooney, C.B.: Atomic-scale variations in contact potential difference on Au/Si(111)-7x7 surface in ultrahigh vacuum. *Appl. Surf. Sci.* **157**, 222 (2000)
24. Glatzel, T., Zimmerli, L., Koch, S., Kawai, S., Meyer, E.: Molecular assemblies grown between metallic contacts on insulating surfaces. *Appl. Phys. Lett.* **94**(6), 063303 (2009)
25. Bocquet, F., Nony, L., Loppacher, C., Glatzel, T.: Analytical approach to the local contact potential difference on (001) ionic surfaces: Implications for Kelvin probe force microscopy. *Phys. Rev. B* **78**, 035410 (2008)
26. Enevoldsen, G., Glatzel, T., Christensen, M., Lauritsen, J., Besenbacher, F.: Atomic scale kelvin probe force microscopy studies of the surface potential variations on the TiO₂(110) surface. *Phys. Rev. Lett.* **100**, 236104 (2008)
27. Meyer, E., Glatzel, T.: Novel probes for molecular electronics. *Science* **324**(5933), 1397–1398 (2009)
28. Zhang, R., Zhang, Y., Dong, Z.C., Jiang, S., Zhang, C., Chen, L.G., Zhang, L., Liao, Y., Aizpurua, J., Luo, Y., Yang, J.L., Hou, J.G.: Chemical mapping of a single molecule by plasmon-enhanced Raman scattering. *Nature* **498**(7452), 82 (2013)
29. Nanolino Group (2015). <http://nanolino.unibas.ch/>
30. Zimmerli, L., Maier, S., Glatzel, T., Gnecco, E., Pfeiffer, O., Diederich, F., Fendt, L., Meyer, E.: Formation of molecular wires on nanostructured KBr. *J. Phys. Conf. Ser.* **61**(1), 1357–1360 (2007)
31. Maier, S., Fendt, L.A., Zimmerli, L., Glatzel, T., Pfeiffer, O., Diederich, F., Meyer, E.: Nanoscale engineering of molecular porphyrin wires on insulating surfaces. *Small* **4**, 1115–1118 (2008)
32. Kawai, S., Maier, S., Glatzel, T., Koch, S., Such, B., Zimmerli, L., Fendt, L.A., Diederich, F., Meyer, E.: Cutting and self-healing molecular wires studied by dynamic force microscopy. *Appl. Phys. Lett.* **95**(10), 103109 (2009)
33. Gross, L., Schlittler, R.R., Meyer, G., Fendt, L.A., Diederich, F., Glatzel, T., Kawai, S., Koch, S., Meyer, E.: Contacting self-ordered molecular wires by nanostencil lithography. *J. Vac. Sci. Technol. B* **28**(3), C4D34–C4D39 (2010)
34. Such, B., Trevelyan, T., Glatzel, T., Kawai, S., Zimmerli, L., Meyer, E., Shluger, A.L., Amijs, C.H.M., de Mendoza, P., Echavarren, A.M.: Functionalized truxenes: Adsorption and diffusion of single molecules on the KBr(001) surface. *ACS Nano* **4**(6), 3429–3439 (2010)
35. Trevelyan, T., Such, B., Glatzel, T., Kawai, S., Shluger, A.L., Meyer, E., de Mendoza, P., Echavarren, A.M.: Organic molecules reconstruct nanostructures on ionic surfaces. *Small* **7**(9), 1264–1270 (2011)
36. Such, B., Glatzel, T., Kawai, S., Koch, S., Meyer, E.: Three-dimensional force spectroscopy of KBr(001) by tuning fork-based cryogenic noncontact atomic force microscopy. *J. Vac. Sci. Technol. B* **28**(3), C4B1–C4B5 (2010)
37. Pawlak, R., Kawai, S., Frey, S., Glatzel, T., Meyer, E.: Atomic-scale mechanical properties of orientated C60 molecules revealed by noncontact atomic force microscopy. *ACS Nano* **5**(8), 6349–6354 (2011)
38. Frey, S., Kawai, S., Pawlak, R., Glatzel, T., Baratoff, A., Meyer, E.: Three-dimensional dynamic force spectroscopy measurements on KBr(001): atomic deformations at small tip-sample separations. *Nanotechnology* **23**(5), 055401 (2012)
39. Pawlak, R., Frey, S., Kawai, S., Glatzel, T., Fang, H., Fendt, L.A., Diederich, F., Meyer, E.: Directed rotations of single porphyrin molecules controlled by localized force spectroscopy. *ACS Nano* **6**(7), 6318–6324 (2012)
40. Pawlak, R., Kawai, S., Frey, S., Glatzel, T., Meyer, E.: J. Phys.: High-resolution imaging of C 60 molecules using tuning-fork-based non-contact atomic force microscopy. *Condens. Matter* **24**(8), 084005 (2012)

41. Such, B., Glatzel, T., Kawai, S., Meyer, E., Turansky, R., Brndiar, J., Stich, I.: Interplay of the tip-sample junction stability and image contrast reversal on a Cu(111) surface revealed by the 3D force field. *Nanotechnology* **23**(4), 045705 (2012)
42. Kawai, S., Pina, C.M., Bubendorf, A., Fessler, G., Glatzel, T., Gnecco, E., Meyer, E.: Systematic study of the dolomite (104) surface by bimodal dynamic force microscopy in ultra-high vacuum. *Nanotechnology* **24**(5), 055702 (2013)
43. Pawlak, R., Glatzel, T., Pichot, V., Schmidlin, L., Kawai, S., Fremy, S., Spitzer, D., Meyer, E.: Local detection of nitrogen-vacancy centers in a nanodiamond monolayer. *Nano Lett.* **13**(12), 5803–5807 (2013)
44. Martin, R.E., Diederich, F.: Linear monodisperse π -conjugated oligomers: model compounds for polymers and more. *Angew. Chem. Int. Ed.* **38**(10), 1350–1377 (1999)
45. Yella, A., Lee, H.W., Tsao, H.N., Yi, C., Chandiran, A.K., Nazeeruddin, M., Diau, E.W.G., Yeh, C.Y., Zakeeruddin, S.M., Grätzel, M.: Porphyrin-sensitized solar cells with cobalt (II/III) based redox electrolyte exceed 12 percent efficiency. *Science* **334**(6056), 629–634 (2011)
46. Cheng, F., Zhang, S., Adronov, A., Echegoyen, L., Diederich, F.: Triply fused Zn^{II}-porphyrin oligomers: synthesis, properties, and supramolecular interactions with single-walled carbon nanotubes (SWNTs). *Chem. Eur. J.* **12**, 6062–6070 (2006)
47. Glatzel, T., Zimmerli, L., Kawai, S., Meyer, E., Fendt, L.A., Diederich, F.: Oriented growth of porphyrin-based molecular wires on ionic crystals analysed by nc-AFM. *Beilstein J. Nanotechnol.* **2**, 34–39 (2011)
48. Yokoyama, T., Yokoyama, S., Kamikado, T., Okuno, Y., Mashiko, S.: Selective assembly on a surface of supramolecular aggregates with controlled size and shape. *Nature* **413**, 619 (2001)
49. Such, B., Czuba, P., Piatkowski, P., Szymonski, M.: AFM studies of electron-stimulated desorption process of KBr(001) surface. *Surf. Sci.* **451**(1–3), 203–207 (2000)
50. Such, B., Kolodziej, J., Czuba, P., Piatkowski, P., Struski, P., Krok, F., Szymonski, M.: Surface topography dependent desorption of alkali halides. *Phys. Rev. Lett.* **85**(12), 2621–2624 (2000)
51. Pšenčík, J., Arellano, J.B., Ikonen, T.P., Borrego, C.M., Laurinmäki, P.A., Butcher, S.J., Serimaa, R.E., Tuma, R.: Internal structure of chlorosomes from brown-colored chlorobium species and the role of carotenoids in their assembly. *Biophys. J.* **91**(4), 1433–1440 (2006)
52. Glatzel, T., Sadewasser, S., Lux-Steiner, M.: Amplitude or frequency modulation-detection in Kelvin probe force microscopy. *Appl. Surf. Sci.* **210**(84), 84–89 (2003)
53. Zahl, P., Bammerlin, M., Meyer, G., Schlittler, R.R.: All-in-one static and dynamic nanostencil atomic force microscopy/scanning tunneling microscopy system. *Rev. Sci. Instrum.* **76**(2), 023707 (2005)
54. Gross, L., Mohn, F., Moll, N., Schuler, B., Criado, A., Guitian, E., Pena, D., Gourdon, A., Meyer, G.: Bond-order discrimination by atomic force microscopy. *Science* **337**(6100), 1326–1329 (2012)
55. Weymouth, A.J., Hofmann, T., Giessibl, F.J.: Quantifying molecular stiffness and interaction with lateral force microscopy. *Science* **343** (6175), 1120–1122 (2014)
56. Fremy, S.: The nature of condensed single molecules—local electronic and mechanical characteristics. Ph.D. thesis, University of Basel (2013)
57. Iancu, V., Deshpande, A., Hla, S.W.: Manipulating kondo temperature via single molecule switching. *Nano Lett.* **6**(4), 820–823 (2006)
58. Lafferentz, L., Ample, F., Yu, H., Hecht, S., Joachim, C., Grill, L.: Conductance of a single conjugated polymer as a continuous function of its length. *Science* **323**(5918), 1193–1197 (2009)
59. Sims, P.C., Moody, I.S., Choi, Y., Dong, C., Iftikhar, M., Corso, B.L., Gul, O.T., Collins, P. G., Weiss, G.A.: Electronic measurements of single-molecule catalysis by cAMP-dependent protein Kinase A. *J. Am. Chem. Soc.* **135**(21), 7861–7868 (2013)
60. Janssen, K.P.F., De Cremer, G., Neely, R.K., Kubarev, A.V., Van Loon, J., Martens, J.A., De Vos, D.E., Roefsaers, M.B.J., Hofkens, J.: Single molecule methods for the study of catalysis: from enzymes to heterogeneous catalysts. *Chem. Soc. Rev.* **43**, 990–1006 (2014)

61. Qu, J., Gao, B., Tian, H., Zhang, X., Wang, Y., Xie, Z., Wang, H., Geng, Y., Wang, F.: Donor-spacer-acceptor monodisperse conjugated co-oligomers for efficient single-molecule photovoltaic cells based on non-fullerene acceptors. *J. Mater. Chem. A* **2**, 3632–3640 (2014)
62. Glatzel, T.: *Measuring Atomic-Scale Variations of the Electrostatic Force*. Springer, Berlin (2011)
63. Fremy, S., Sadeghi, A., Baratoff, A., Goedecker, S., Glatzel, T.: Submitted for publication (2014)
64. Stadtmüller, B., Kröger, I., Reinert, F., Kumpf, C.: Submonolayer growth of CuPc on noble metal surfaces. *Phys. Rev. B* **83**, 085416 (2011)
65. Mugarza, A., Robles, R., Krull, C., Korytár, R., Lorente, N., Gambardella, P.: Electronic and magnetic properties of molecule-metal interfaces: transition-metal phthalocyanines adsorbed on Ag(100). *Phys. Rev. B* **85**, 155437 (2012)
66. Schaffert, J., Cottin, M.C., Sonntag, A., Karacuban, H., Bobisch, C.A., Lorente, N., Gauyacq, J.P., Möller, R.: Imaging the dynamics of individually adsorbed molecules. *Nat. Mater.* **12**(3), 223–227 (2013)
67. Schaffert, J., Cottin, M.C., Sonntag, A., Bobisch, C.A., Möller, R., Gauyacq, J.P., Lorente, N.: Tunneling electron induced rotation of a copper phthalocyanine molecule on Cu(111). *Phys. Rev. B* **88**, 075410 (2013)

Imaging and Manipulation of Adsorbates Using Dynamic
Force Microscopy

Proceedings from the AtMol Conference Series,

Nottingham, UK, April 16-17, 2013

Moriarty, P.; Gauthier, S. (Eds.)

2015, XX, 154 p. 62 illus., 40 illus. in color., Hardcover

ISBN: 978-3-319-17400-6